

# Computational spectroscopy of helium-solvated molecules: effective inertia, from small He clusters toward the nano-droplet regime

Stefano Paolini,<sup>1,2,\*</sup> Stefano Fantoni,<sup>1,2,†</sup> Saverio Moroni,<sup>2,‡</sup> and Stefano Baroni<sup>1,2,§</sup>

<sup>1</sup> SISSA – Scuola Internazionale Superiore di Studi Avanzati, via Beirut 2-4, 34014 Trieste, Italy

<sup>2</sup> INFN-DEMOCRITOS National Simulation Center, Trieste, Italy

(Dated: January 3, 2022)

Accurate computer simulations of the rotational dynamics of linear molecules solvated in He clusters indicate that the large-size (nano-droplet) regime is attained quickly for light rotors (HCN, CO) and slowly for heavy ones (OCS, N<sub>2</sub>O, CO<sub>2</sub>), thus challenging previously reported results. Those results spurred the view that the different behavior of light rotors with respect to heavy ones—including a smaller reduction of inertia upon solvation of the former—would result from the lack of *adiabatic following* of the He density upon molecular rotation. We have performed computer experiments in which the rotational dynamics of OCS and HCN molecules was simulated using a fictitious inertia appropriate to the *other* molecule. These experiments indicate that the approach to the nano-droplet regime, as well as the reduction of the molecular inertia upon solvation, is determined by the anisotropy of the potential, more than by the molecular weight. Our findings are in agreement with recent infrared and/or microwave experimental data which, however, are not yet totally conclusive by themselves.

PACS numbers: 36.40.-c, 34.20.+h, 67.40.Yv, 36.40.Mr, 02.70.Ss

## INTRODUCTION

The recent discovery that small molecules solvated in He clusters display a sharp rotational spectrum with well resolved lines is a spectacular manifestation of He superfluidity in such extreme confined conditions [1, 2]. Recent developments in quantum many-body simulation techniques are allowing for the determination of the first few excited states of interacting boson systems [3, 4, 5], as well as for an understanding of the relations existing between structure, dynamics, and superfluidity in these systems [6, 7]. In particular, it has now become possible to *predict* the dependence of the effective molecular rotational constant,  $B$ , on the cluster size,  $N$ , for clusters up to a few tens of He atoms [8].

Results based on the so-called *projection operator imaginary-time spectral evolution* (POITSE, an implementation of diffusion quantum Monte Carlo aimed at estimating excitation energies) provide the following scenario for the dependence of  $B$  upon  $N$  [7, 9, 10]: *i*) the inertia of heavy rotors is reduced by a factor 2-3 upon solvation, whereas the reduction is of the order of a few tens percent only in the case of light molecules; *ii*) the inertia of solvated heavy rotors (such as, *e.g.*, OCS or SF<sub>6</sub>) would reach the large-size (nano-droplet) regime well before the first solvation shell is completed, whereas the convergence for light rotors would be much slower. This scenario was partially rationalized using the concept of *adiabatic following*. Heavy molecules rotate slowly when excited and they usually have a stronger and more asymmetric interaction potential with the surrounding He atoms. As a result of the combination of these two effects, a fraction of the He solvent density would be dragged along by the rotation of the molecule, thus contributing to in-

crease its inertia. This effect would be greatly reduced in light rotors both because they rotate faster, and because their interaction with He atoms is usually more spherical. Both these facts hinder the dragging of He atoms, in qualitative agreement with experiments which positively support the first of the above two findings. The fact that only a fraction of the He density in the first solvation shell would adiabatically follow the molecular rotation would explain the alleged fast convergence of the molecular inertia to the nano-droplet regime for heavy rotors [9, 10]. The alleged slow convergence for light rotors would instead be due to the interaction between molecular rotation and bulk-like collective excitations that is supposed to occur for large enough clusters [9, 24, 26]. Experimental results often exist only for large clusters. Some results on small clusters begin to be available, but data in the intermediate regime are not yet sufficient to validate this picture.

In this paper this problem is re-addressed using *Rep-tation Quantum Monte Carlo* (RQMC), a method that we believe to be the most appropriate existing to date to study the dynamical properties of interacting boson systems [3, 4]. As paradigmatic cases of heavy and light solvated molecular rotors we choose OCS@He<sub>N</sub> and HCN@He<sub>N</sub>, respectively. In order to disentangle the role of the bare molecular inertia from that of the potential anisotropy, we have performed computer experiments in which the rotational dynamics of OCS and HCN molecules was simulated using a fictitious inertia appropriate to the *other* molecule. These experiments indicate that the approach to the nano-droplet regime, as well as the reduction of the molecular inertia upon solvation, is determined by the anisotropy of the potential, more than by the molecular weight.

Our paper is organized as follows. In Sec. II we briefly review our theoretical framework. Sec. III.A contains our results for  $\text{OCS@He}_N$  which considerably extend the size range considered in a previous publication [6]. We also address the problem of the accuracy of the molecule-He interaction potential [11] and we show that avoiding the *morphing* procedure followed to brush up the potential, allows for a much better (actually, almost perfect) agreement between simulations and rotational spectroscopy experiments. In Sec. III.B we present results of similar simulations made for  $\text{HCN@He}_N$ . In Sec. III.C we present computer experiments done on molecules with *fudged* masses (*i.e.* by using the inertia of one molecule and the interaction potential of the other), and we discuss the implications of these results on the main issue raised in the present paper (*i.e.* the relative importance of the bare molecular inertia and of the anisotropy of the molecule-atom potential in determining the rotational properties of solvated molecules, as a function of the cluster size). Finally, Sec. IV contains our conclusions.

## THEORY

We consider a realistic Hamiltonian in which  $N$  He atoms are treated as point particles interacting via a pair potential, and the dopant molecule (either OCS or HCN) as a rigid linear rotor, with only translational and rotational degrees of freedom. Both the He-He and the He-molecule interactions are parametrized after accurate ab-initio quantum chemistry calculations [11, 12, 13]. For the He-OCS potential energy surface (PES), in particular, we use the *unmorphed* version of Ref. 11. In the next section we show that this version—which results from a direct fit to quantum-chemistry calculations—is considerably more accurate for a wide range of cluster sizes [8] than the *morphed* one which was refined so as to improve the predictions for the spectrum of the  $\text{OCS@He}_1$  complex [11]. Contour plots of the He-HCN and the He-OCS PES are displayed in Fig. 1, showing a much greater strength and anisotropy of the latter.

We simulate the system using the RQMC method [3, 4]. Details of the calculations are similar to those of previous studies for  $\text{OCS@He}_N$  and  $\text{CO@He}_N$  clusters [6, 16]. Briefly, the imaginary-time evolution operator projects a state defined by a trial function  $\Phi_0$  onto  $|\Phi(\beta)\rangle = \exp(-\beta\hat{H})|\Phi_0\rangle$ , which in turn approaches the exact ground state,  $\Psi_0$ , as  $\beta$  goes to infinity. Expectation values on  $|\Phi(\beta)\rangle$ ,  $\langle\Phi(\beta)|\hat{O}|\Phi(\beta)\rangle/\langle\Phi(\beta)|\Phi(\beta)\rangle$ , are computed using a discretized path-integral representation of the imaginary-time evolution, which becomes exact in the limit of zero time step. The resulting paths are sampled with an efficient generalized Metropolis algorithm. The average  $\langle\hat{O}\rangle$  of the values taken by the operator  $\hat{O}$  on the sampled paths gives an estimate of the desired expectation value within a known statistical error and

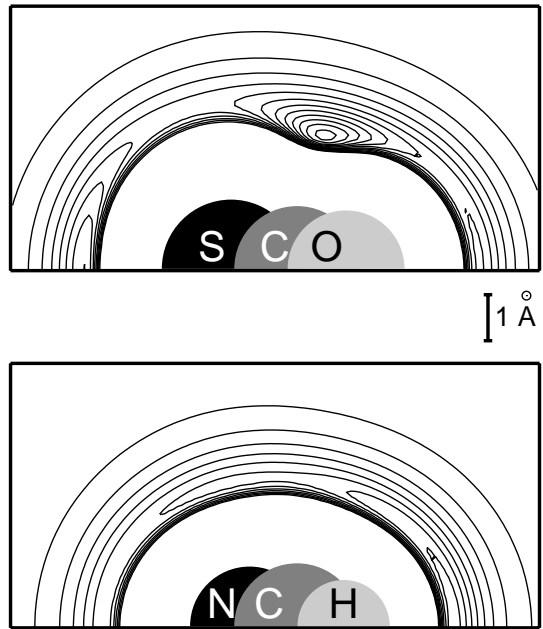


FIG. 1: Potential energy surfaces of He-OCS (up) and He-HCN (down) used in this work. The He-OCS PES is the *unmorphed* version from Ref. 11 (see text). Contour levels start from  $V = 0$  to negative values, and they are spaced by  $5^\circ\text{K}$ . The He-OCS interaction potential has a deep *equatorial* doughnut-shaped well around the C atom, and two secondary *polar* minima in correspondence of the O and S atoms, the one at the S pole being broader and deeper. The He-HCN interaction potential, instead, has a shallow main minimum in correspondence of the hydrogen molecular pole and an even shallower secondary one slightly below the equator on the nitrogen side, the latter being barely visible in the figure.

without any mixed-estimate nor population-control biases. Here  $\hat{O}$  can be either a static operator (such as the Hamiltonian itself or the atomic number density distribution) or a time-dependent one (such as those needed to calculate time-correlation functions:  $\hat{A}\exp(-\tau\hat{H})\hat{B}$ ). A single path thus entails the imaginary-time evolution of the system for a total time  $2\beta + \tau$ , which in our simulations is typically between 1 and 2 inverse K, with a discretization time step,  $\epsilon$ , of  $10^{-3} \text{ K}^{-1}$ . By explicitly checking the convergence of the results to the limits of large projection time and zero time step, we make sure that the computed quantities accurately represent their ground state values.

The trial function is taken of the Jastrow form,

$$\Phi_0 = \exp \left[ - \sum_{i=1}^N u_1(r_i, \theta_i) - \sum_{i < j}^N u_2(r_{ij}) \right], \quad (1)$$

where  $\mathbf{r}_i$  is the position of the  $i$ -th atom with respect to the center of mass of the molecule,  $r_i = |\mathbf{r}_i|$ ,  $\theta_i$  is the

angle between the molecular axis and  $\mathbf{r}_i$ , and  $r_{ij}$  is the distance between the  $i$ -th and the  $j$ -th He atoms. On account of the anisotropy of the PES, the He-molecule pseudo-potential,  $u_1$ , is expressed as a sum of products of Legendre polynomials times radial functions. Retaining five or six terms in the sum is enough to represent even the most anisotropic situation, namely a ring of up to 5 He atoms tightly bound around the OCS molecular axis in correspondence of the principal minimum of the PES. The choice of the radial functions is not critical, as soon as their variational parameters ensure sufficient flexibility in the relevant range of He-molecule distances. The resulting variational parameters, whose number is in the range of several tens, are optimized by minimizing the variational energy with the variational Monte Carlo method.

Information on the rotational excitations of the cluster can be obtained from the imaginary time autocorrelation functions [6]:

$$c_J(\tau) = \langle P_J(\mathbf{n}(\tau) \cdot \mathbf{n}(0)) \rangle, \quad (2)$$

where  $\mathbf{n}$  is the molecular orientation versor, and  $P_J$  is the Legendre polynomial of degree  $J$ . A generic imaginary-time correlation function can be represented as a linear combination of exponentials, whose decay constants are the excitation energies of the system, and whose coefficients are the corresponding oscillator strengths. The usefulness of this representation for obtaining dynamical properties from quantum simulations is in general rather limited. This is so because the calculation of a spectrum from imaginary-time correlations entails carrying out an inverse Laplace transform, a notoriously ill-conditioned problem [17]. In the present case, however, the situation is not as bad because very few excited states contribute to  $c_J(\tau)$ . In fact, if the solvated molecule were isolated, only one rotational state would contribute to  $c_J(\tau)$  which would therefore have the form of a single exponential. Furthermore, the interaction between the solvent matrix and the soluted molecule is rather weak, so that this single-exponential picture is only slightly perturbed. Last, and most important, the bosonic nature of the quantum solvent determines a low density of low-energy excitations. As a consequence of the scarcity of low-lying excitations available to couple with the molecular rotation, it is thus possible to reliably extract their energies by a multi-exponential fit. A more general analysis, based on the maximum entropy method, gives equivalent results [14].

## RESULTS AND DISCUSSION

### Carbonyl sulfide

Carbonyl sulfide (OCS) appears to have a special role in the spectroscopy of He-solvated molecules. OCS

was used as a microscopic rotor to probe the superfluidity of He nano-droplets in a celebrated *microscopic Andronikashvili experiment* [1]. As a consequence of the paucity of low-lying excitations in the bosonic host, molecular rotational lines are exceedingly sharp and well resolved when the molecule is solvated in  $^4\text{He}$ , while they are broad and unresolved in  $^3\text{He}$ . In the former case the rotational spectrum is well represented by a quasi-rigid free-rotor model:

$$E_J = BJ(J+1) - DJ^2(J+1)^2, \quad (3)$$

where  $B$  is the effective rotational constant of the molecule—renormalized by the interaction with the host to a value smaller but of the same order as in the gas phase—and  $D$  is the rotational distortion constant which is several orders of magnitudes larger than for the free molecule.

A few years later, size-resolved rotational and vibrational spectra of small ( $N = 1 \div 8$ ) OCS@He $_N$  clusters appeared [2], indicating that fingerprints of superfluidity can be identified in clusters as small as  $N = 8$ . These findings spurred a burst of theoretical research aimed at elucidating the relations existing among structure, dynamics, and superfluidity in these small clusters [6, 7]. A semi-quantitative agreement between POITSE results from diffusion quantum Monte Carlo simulations and experiments was reported in Ref. 7 in the size range  $N = 1 \div 8$  (a minimum in the rotational constant was predicted for  $N = 6$ , while experiments show a decrease up to the largest resolved size,  $N = 8$ ), while for  $N > 6$  a fast convergence to the nano-droplet limit was observed (full convergence was claimed to be achieved for  $N = 20$ ). A better agreement was found in Ref. 6, in that the minimum of the rotational constant (located at a cluster size  $N = 8$ ) was found to be compatible with spectroscopic data. Results were also presented for the rotational distortion constant,  $D$ , which was found to reach a minimum for  $N = 5$ , in agreement with experimental findings [2]. In addition, a detailed analysis—based on a comparison between the structure of the clusters and the He-OCS angular-current correlations—allowed to shed light on the microscopic mechanisms responsible for superfluidity.

### Appraising the quality of intermolecular potentials

Much of the discrepancy between the results of quantum Monte Carlo simulations and experiments (as well as *among* different simulations, we should add) may be due to the quality of the He-molecule potential utilized for the simulations [6]. In Ref. 14 it was in fact shown that the difference between the predictions of Refs. 6 and 7 is indeed (almost) entirely due to the poorer quality of the potential utilized in Ref. 7 [15]. In Fig. 2 we compare the atomic density distributions of OCS@He $_8$  and

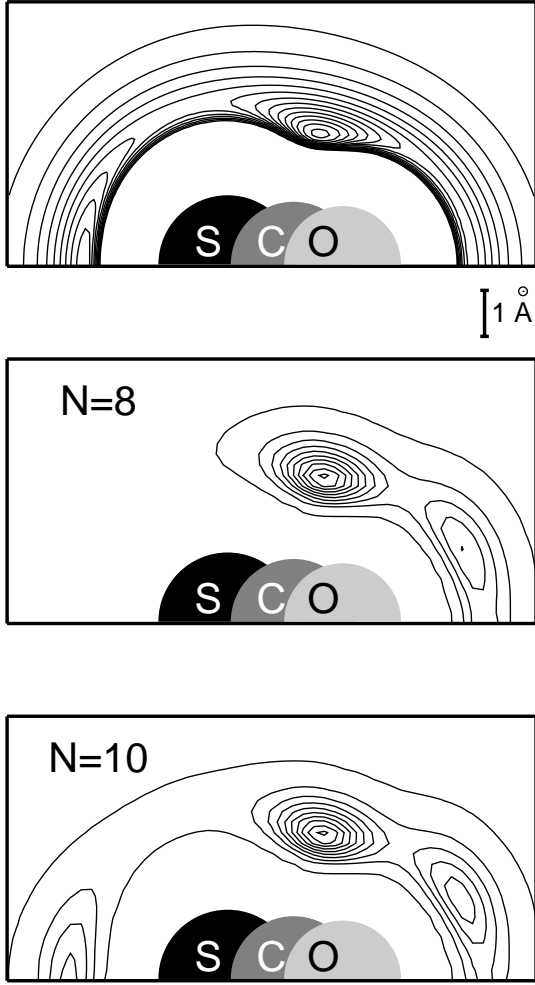


FIG. 2: Upper panel: potential energy surface of He-OCS (we display here the *morphed* version from Ref. 11 which was used in our previous study [4]). Lower panels: contour plots of the helium density profiles of OCS@He<sub>8</sub> and OCS@He<sub>10</sub>. For the density profiles, contour levels start from 0.001 with increments of 0.005, in units of  $\text{\AA}^{-3}$ .

OCS@He<sub>10</sub> with the OCS-He potential used in Ref. 6. According to the analysis of Ref. 6, the minimum in the effective inertia of the solvated OCS molecule occurs at the largest cluster size at which quantum tunneling between the main, *equatorial*, and the two secondary, *polar*, potential wells is hindered by the energy barriers which separate them. It is clear that the larger the barrier, the smaller the tunneling, and the larger the corresponding effective inertia will be. In Ref. 6 it was indeed found that fudging the OCS-He PES—so as to enhance the potential energy barrier which separates the main well from the molecular poles—hardly affects the rotational constant for  $N \leq 5$ , while it increases the inertia for  $N = 6, 7, 8$ , thus bringing the results of the simulations

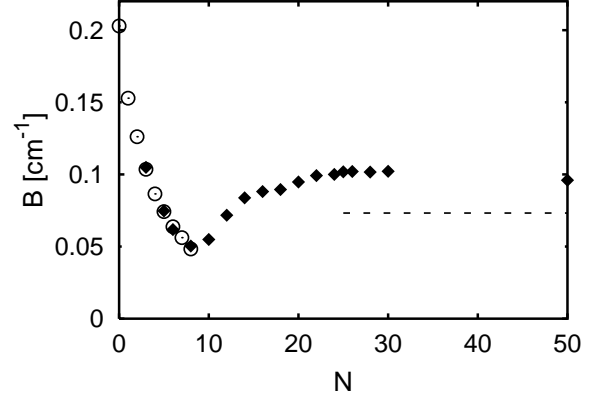


FIG. 3: Effective rotational constant of OCS@He<sub>N</sub>, as a function of the cluster size,  $N$ . Full diamonds: results from RQMC simulations performed using the unmorphed potential of Ref. 11 (see text). Open circles: experimental data from Ref. 2. The horizontal dashed line indicates the nano-droplet limit measured in Ref. 2.

in much better agreement with experiments. It was later found that this too low a value for the relevant energy barriers is in fact an artifact of the *morphing* procedure adopted in Ref. 11, so as to bring an already very accurate OCS-He potential obtained from coupled-cluster quantum-chemical calculations into an even better agreement with the known spectra of the OCS@He<sub>1</sub> complex. Such spectra depend on the details of the potential around the minimum more than on the height of the barriers which separate inequivalent minima. The latter, instead, are expected to crucially affect the properties of the cluster when the main potentials well starts to be filled by He atoms ( $N \geq 5$ , in the present case). We conclude that the spectra of clusters with many He atoms—which depend on the PES far from the minimum—are a much more sensible benchmark of the quality of the PES than those of the helium-molecule dimer. A similar conclusion was drawn in Ref. 14 where a different He-OCS PES was proposed, such that the rotational constants calculated from POITSE simulations agreed well with experimental data available for  $N \leq 8$ . RQMC simulations performed with this PES in the size range  $10 \lesssim N \lesssim 30$  show a behavior of the rotational constant very similar to that reported in Fig. 3, obtained from the *unmorphed* version of the PES of Ref. 11, although the resulting values are slightly smaller for the largest sizes (hence closer to the experimental nano-droplet regime: see below).

#### Effective rotational constants

In Fig. 3 we report the dependence of the effective rotational constant,  $B$ , on the cluster size,  $N$ , as calculated with the unmorphed He-OCS potential of Ref. 11. The



nano-droplet limit resulting from measurements on clusters of  $\approx 6000$  atoms [1] is indicated by a dashed line. Our results compare favorably with experimental data which are available up to  $N = 8$  [2]. In the small-size regime ( $N \leq 8$ ) the rotational constant decreases with increasing cluster size because the He atoms trapped in the (*equatorial*) and in the first *polar* (near oxygen) well are dragged along by the molecular rotation, thus increasing the effective inertia. For  $N > 8$ —as the second *polar* (near sulphur) well starts to be filled—an increasing fraction of the He atoms can freely tunnel among different wells, thus not contributing to the molecular inertia. The quantum fluid nature of the He solvent is such that tunneling is a collective process in which not only the excess atoms not fitting in the main potential well take part, but even those which are tightly bound to it. For this reason, once tunneling among different wells is made possible by the spill-out of excess atoms, this process determines a decrease of the molecular inertia, *i.e.* an increase of the rotational constant for an increasing cluster size. As a matter of fact, it was shown in Ref. 6 that the value of the correlation between the molecular angular momentum and the atomic angular current—which is maximum in the main *equatorial* potential well—starts decreasing as the rotational constant increases past the minimum ( $N > 8$ ). This decrease continues until the first solvation shell is completed at a cluster size  $N \approx 20$ , around which the rotational constant seems to stabilize. As the second solvation shell starts to build, however, quantum exchange cycles involving atoms from this shell would contribute to further, although weakly, decrease the molecular inertia. A similar behavior of the evolution of the rotational constant for sizes shortly beyond completion of the first shell is also observed in simulations of clusters doped with  $N_2O$  and  $CO_2$  [18, 19], which are all molecules having a qualitatively similar interaction with He atoms. Our findings demonstrate that—contrary to a commonly accepted assumption—He atoms from outer (larger than the first) solvation shells do affect the molecular inertia. For  $N_2O$  and  $CO_2$  this is also supported by experimental evidence [20, 21]: the measured value of  $B$  for the largest cluster with secure assignment of spectral lines ( $N = 12$  for  $N_2O$  and  $N = 17$  for  $CO_2$ ) is significantly higher than the nano-droplet limit, with no plausible signs of convergence within the first shell. A role of outer shells in bringing down the effective rotational constant is thus to be expected. How far from the molecule does this effect extend, our simulations—which are limited at present to a few tens of atoms—cannot say yet. This finding is at least compatible with current phenomenological models of the inertia of He-solvated molecules, which predict a lower contribution of the solvent to the molecular inertia, with decreasing atomic density. In hydro-dynamical models a lower atomic density would determine a reduced kinetic energy of the irrotational flow of the solvent; in a two-fluid model, instead, a

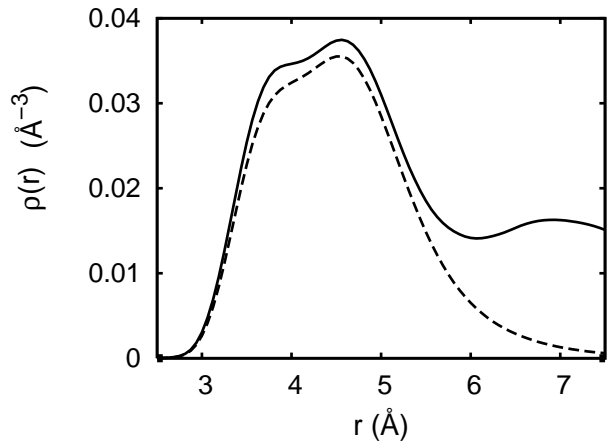


FIG. 4: Radial density profile  $\rho(r)$  of He in  $OCS@He_N$  for  $N = 20$  (dashed line) and  $N = 50$  (solid line).

lower inertia would simply follow from a reduction of the non-superfluid component of the atomic density. Coming down from the nano-droplet regime, a decrease of the atomic density in the first solvation shell(s) is indeed expected, as a consequence of the reduced pressure exerted by the outer shells. This is clearly demonstrated in fig. 4 in which the He radial density profiles around OCS are compared for  $N = 20$  and  $N = 50$ . The radial density in the first shell is significantly lower for the smaller cluster. On purely classical grounds, a competing effect could arise if the spatial extension of the first shell was sensitive to the pressure release, thus affecting the second moments of the atomic density. The density profiles shown in Fig. 4 however suggest that this effect is small, since the positions of the peaks in the first shell hardly change between clusters of 20 and 50 He atoms.

Our results demonstrate that in  $OCS@He_N$  clusters the effective rotational constant does not attain its asymptotic limit upon completion of the first solvation shell, being in fact higher at this size. When the second shell starts to build up, the value of  $B$  further increases (arguably, via quantum exchange cycles involving particles of both shells [18, 22]). Whether, in larger clusters, the missing inertia will be recovered by a change in the density of the first shell or by a direct contribution from the outer shells, or both, remains to be investigated.

### Hydrogen cyanide

Hydrogen cyanide (HCN) is considered as a prototype of light helium-solvated rotors [9, 10], for which the assumption of *adiabatic following* breaks down. This has been demonstrated both experimentally, by comparing the rotational constants of HCN and DCN in the nano-droplet regime [23], and theoretically, by comparing the

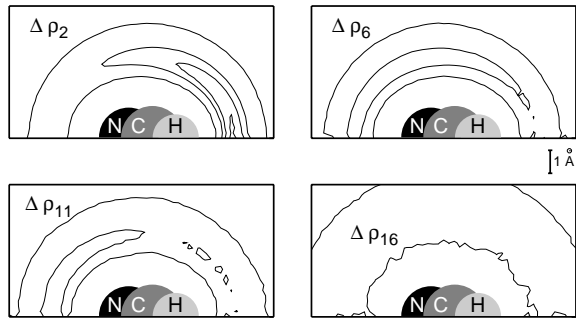


FIG. 5: Contour plot of the incremental density,  $\Delta\rho_N(\mathbf{r}) = \rho_N(\mathbf{r}) - \rho_{N-1}(\mathbf{r})$ , for selected HCN@He $_N$  clusters. The HCN molecule has its center of mass at the origin, with the hydrogen atom on the positive  $x$  direction. Distances are in Å, and contour levels start from 0.0001 with increments of 0.001, in units of inverse cubic Å.

He density profiles obtained from simulations performed including and, in turn, neglecting the molecular degrees of freedom [24]. The calculation of the molecular rotational constant,  $B$ , in large droplets thus defies the application of either the two-fluid [9] and hydrodynamic models [25], which both rely on *adiabatic following*, albeit in a different manner. On the other hand, direct calculation of rotational excitations by the POITSE method [24] indicated that the nano-droplet value would not be reached even for  $N = 25$ , well beyond completion of the first solvation shell. This slow convergence of the rotational constant as a function of the cluster size was later attributed to the coupling of molecular rotation to phonon-like excitations of the solvent which would develop only in the nano-droplet regime [26]. Unfortunately experimental data for the effective rotational constant of HCN are only available, so far, for very large droplets [23]. We will see however how a comparison of our theoretical results for HCH@He $_N$  with both theoretical and experimental results which are available for the closely related CO@He $_N$  system will allow to draw a number of important and non trivial conclusions.

### Structural properties

In Fig. 5 we report the incremental atomic density profile of HCN,  $\Delta\rho_N(\mathbf{r}) = \rho_N(\mathbf{r}) - \rho_{N-1}(\mathbf{r})$ , as calculated for a few selected cluster sizes. For the binary complex, HCN@He $_1$ , the He density forms a broad cap around the H end of the HCN molecule, centered on the main well of the PES. As  $N$  increases, the He density smoothly piles up with no visible signature of the secondary, *sub-equatorial*, minimum. The incremental density is mainly localized on the H side of the HCN molecule for  $N$  up to 6, mainly on the N side for  $N$  between 8 and 14, and nearly

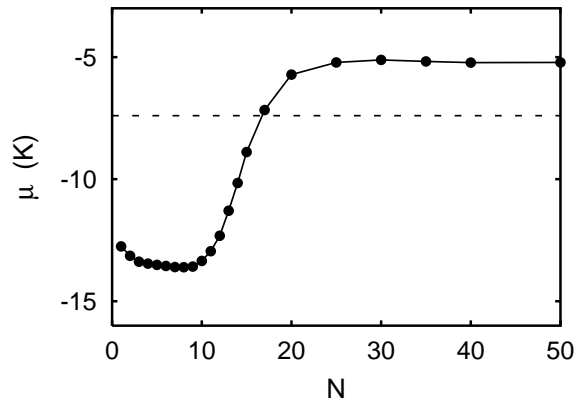


FIG. 6: Chemical potential,  $\mu(N) = E(N) - E(N - 1)$ , for HCN@He $_N$  clusters. The dashed line is the bulk limit.

isotropically thereafter. Starting from  $N$  around 16, the incremental density shifts toward larger distances from the HCN center of mass (see the inner and the outer contour levels in Fig. 5). We consider this behavior as an indication that the first solvation shell is completed around  $N \approx 15$ , although shell effects are by no means sharp in this system (for instance, much more pronounced effects are seen at  $N = 12$  in clusters of para-hydrogen seeded with HCN [29, 30]).

The dependence of the cluster ground-state energy,  $E(N)$ , on the size of the system reflects the extremely smooth evolution of the He density profile, as shown in Fig. 6 which reports the chemical potential,  $\mu(N) = E(N) - E(N - 1)$ . For  $N$  up to a dozen the effects of the He-HCN interaction dominates: the chemical potential stays almost constant, decreasing only very weakly with the cluster size, as a consequence of the He-He interaction. For  $12 \lesssim N \lesssim 20$  the first solvation shell is filled and the kinetic energy of He atoms increases due to their closer packing, thus determining a rise of the chemical potential. For  $N \gtrsim 20$   $\mu(N)$  is stabilized again at value which is higher than the bulk limit, due to the smaller effects of the He-He interaction in this size range.

The fact that the first solvation shell is completed in the size range  $12 \lesssim N \lesssim 20$  is confirmed by an analysis of the angular correlations of He atom pairs. Let us define the He-He pair distribution of the dihedral angle with respect to the molecular axis,  $\phi$ , as:

$$C(\phi) = \frac{1}{N(N-1)} \left\langle \sum_{i < j} \delta(\phi - \phi_i + \phi_j) \right\rangle. \quad (4)$$

$C(\phi)$  gives a measure of the (weak) tendency of the He atoms to cluster together on the same side of the molecular axis, due to the He-He attraction [16]. The integrated

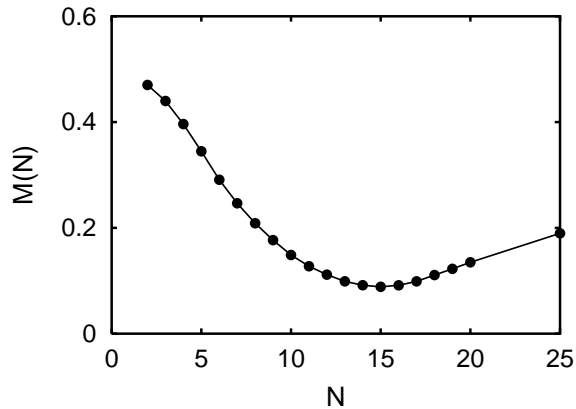


FIG. 7: Integrated pair distribution of the dihedral angle, defined in Eq. 5, as a function of the cluster size, for  $\text{HCN@He}_N$ .

quantity,

$$M = \int_0^{\pi/2} C(\phi) d\phi - 1/2, \quad (5)$$

displayed in Fig. 7 as a function of  $N$ , reveals that this tendency is smallest around  $N = 15$ , corresponding to completion of the first solvation shell where, for steric reasons, the angular distribution of He atoms around the molecule is most uniform.

#### Rotational excitations

All the above features of He-solvated HCN molecules are similar to the CO case, already studied in a previous work [16]. In Fig. 8 we report the energies of the two lowest rotational excitations with angular momentum  $J = 1$ , along with the corresponding spectral weights. We note that our predictions for  $N > 10$  considerably differ from those of Ref. 24 which were obtained with the POITSE method. We cannot offer any explanation for this discrepancy. We can only observe that the value of  $B$  calculated in Ref. 24 for  $N = 25$  is even larger than in the gas phase, a fact that can hardly be explained on physical grounds. In fact, while the reduction of one of the moments of inertia below its value in gas phase—experimentally observed in the binary complex—can be explained by the considerable relative mass redistribution occurring upon formation of the binary complex, similar effects are hard to justify at cluster sizes where the density profile evolves with  $N$  in a smooth and almost isotropical way. This seems to suggest that the results of Ref. 24 may be affected by some inaccuracies for the largest sizes considered in that work. On the other hand, while it is difficult, for large cluster sizes, to ensure full convergence with respect to projection time, as

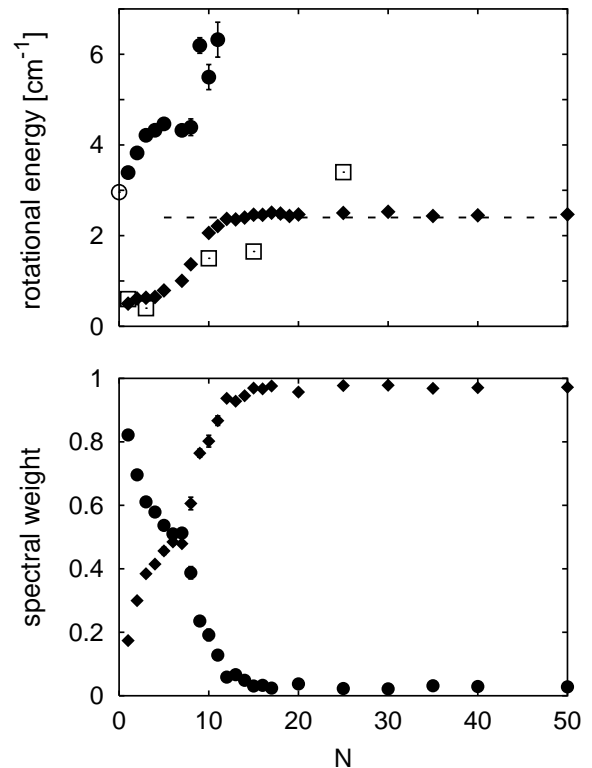


FIG. 8: Upper panel: Rotational energies of  $\text{HCN@He}_N$  as functions of the cluster size, computed by RQMC (*a*-type, diamonds and *b*-type, filled circles); results from the POITSE calculations of Ref. 24 are indicated by squares. The dashed line is the effective rotational constant of HCN in the nano-droplet limit[23], while the empty circle at  $N = 0$  is the gas-phase value. Energy units are  $\text{cm}^{-1}$ . Lower panel: Spectral weight of the *a*-type line (diamonds) and the *b*-type line (filled circles).

well as full ergodicity in path sampling, we note that the present calculations for HCN are indirectly supported by the agreement between the experiment [27] and similar calculations for the closely related CO-He clusters [16].

Two series of excitations, called *a*-type and *b*-type lines, evolve smoothly from the known *end-over-end* and the *free molecule* rotational modes of the binary complex, respectively. The *b*-type line starts off with a stronger spectral weight, then it quickly weakens and eventually disappears. Note how the intensity of the *b*-type line follows the decline of the He-density anisotropy displayed in Fig. 7. The existence of two relevant spectral lines (instead of a single line appropriate to the spectrum of a linear rotor) is in fact a manifestation of the dynamical anisotropy of the atomic-density distribution around the molecular axis, which lowers the cylindrical symmetry of the molecular rotor. For  $N > 15$  the rise of the He-density anisotropy does not give rise to any significant line splitting because it is due to atoms in the second sol-

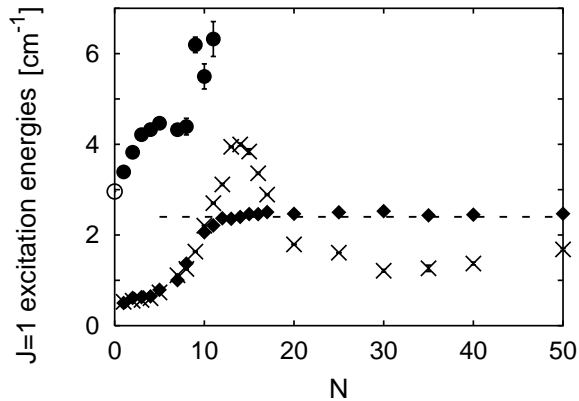


FIG. 9: Comparison between the positions of the spectral lines reported in Fig. 8 with the lowest mode in the spectral resolution of the correlation  $\gamma(t)$ .

vation shell, which are only very weakly coupled to the molecular rotation.

The coupling between the molecular rotation and He-density fluctuations is best understood using the (imaginary) time correlations of the vector,  $\mathbf{u}$ , pointing from the molecular center of mass towards the center of mass of the complex of He atoms. Such a time correlation function,  $\gamma(t) = \langle \mathbf{u}(0) \cdot \mathbf{u}(t) \rangle$ , contains information on the energies and spectral weights of the  $J = 1$  cluster excitations whose character is predominantly that of a He-density fluctuation. In Fig. 9 we display the lowest-lying excitation energy extracted from the spectral resolution of  $\gamma(t)$  as a function of the cluster size, and compare it with the positions of the *a*-type and *b*-type lines already reported in Fig. 8. We see that this density-fluctuation excitation—which has a relatively strong spectral weight—is degenerate with the *a*-type line for  $N \lesssim 10$ . This mode has been interpreted as a cluster excitation in which part of the He density is dragged along by the molecular rotation [16]. This interpretation is trivial for the binary complex (it corresponds to the end-over-end rotation), but it has no obvious visualization for larger clusters. For  $N > 10$ , the energy of this mode departs from the *a*-type line, and the *b*-type line correspondingly disappears. This relates to the onset of a situation where the He density is decoupled from the molecular rotation.

We come now to the main concern of this paper, *i.e.* the convergence of the effective rotational constant to its asymptotic, large-size, value. Our results indicate that the residual renormalization of the effective inertia does not change significantly upon further growth of the cluster beyond, say,  $N = 15$ . This fact is in complete analogy with the findings reported in Ref. 16 for clusters doped with CO (and in agreement high resolution IR spectra recently obtained for He clusters seeded with CO up to  $N = 20$  [27]), but at variance with the results reported

for HCN in Ref. 24 and with a commonly accepted view. With a similar rotational constant and a similar interaction with He, CO and HCN are not expected to behave very differently upon solvation in He clusters. The experimental results for CO do not seem compatible with a large variation of  $B$  between, say,  $N = 15$  and 25, thus challenging the idea of slow convergence to the nano-droplet limit as a general feature of the effective inertia of quantum solvated light rotors. Although a conclusive answer will require the measurement and assignment of spectral lines for even larger clusters, we believe that the agreement between our previous calculations and high-resolution IR measurements for the closely related  $\text{CO@He}_N$  system warrants a considerable trust in the present results and in the conclusions on the approach to the nano-droplet regime based on them.

In conclusion, the results reported here for HCN and in Refs. 16 for CO (the latter being supported by the experimental study of Ref. 27) suggest that for these *light rotors* the asymptotic value of the effective rotational constant is reached well before completion of the first solvation shell. We will see in the next Section that this behavior is better attributed to the weak anisotropy of the potential, rather than to the small value of  $B$  in gas phase.

### Fudged molecules

In this section we consider the fractional reduction of the gas-phase rotational constant  $B_0$  upon solvation in He nano-droplets,  $\Delta = B/B_0$ . The observed general trend (see e.g. Fig. 13 in Ref. 10) is that lighter rotors tend to have larger values of  $\Delta$ . A suitably defined *amount of adiabatic following* [31] has been proposed as the key physical property responsible for the value of  $\Delta$ . Qualitatively, the analysis of Ref. 31 supports the simple picture that both a small molecular inertia and a weakly anisotropic interaction lead to a large value for  $\Delta$ . However, there are several exceptions: for instance,  $\text{N}_2\text{O}$  has  $B_0 = 0.30$  K and  $\Delta = 0.17$ , whereas OCS (a *typical entry* in the mentioned general trend) has  $B_0 = 0.15$  K and  $\Delta = 0.36$ . Given that for OCS there is *saturation* to almost full *adiabatic following*, [31] the significantly smaller  $\Delta$  value for  $\text{N}_2\text{O}$  cannot be explained by resorting to the concept of *adiabatic following* alone. Therefore, it seems useful to gain further insight by disentangling the role of the PES anisotropy from that of the gas-phase inertia. To this purpose, we have performed simulations with two fictitious molecules: f-OCS (*fudged* OCS), with the PES as OCS and the same  $B_0$  value as HCN, and f-HCN (*fudged* HCN), featuring the HCN-He interaction and the  $B_0$  value of OCS. Note that the gas-phase rotational constants of OCS and HCN are in a ratio of about 1:7.

The rotational energies of f-OCS@He $_N$  are shown in Fig. 10, and the corresponding spectral weights in Fig. 11.



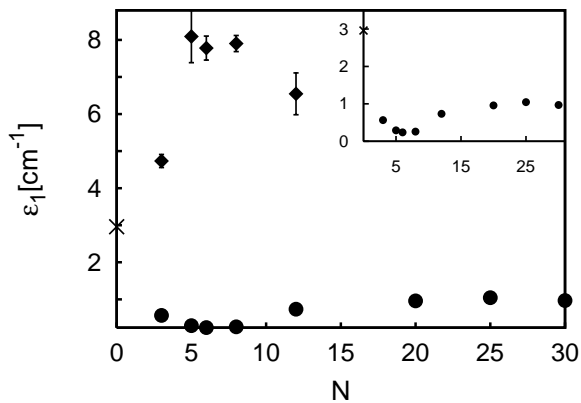


FIG. 10: Rotational energies of f-OCS@He<sub>N</sub> as a function of the cluster size (*a*-type, filled circles, and *b*-type, diamonds). The cross at  $N = 0$  shows the fictitious value of  $2B_0$ . Inset: the detail of the *a*-type line.

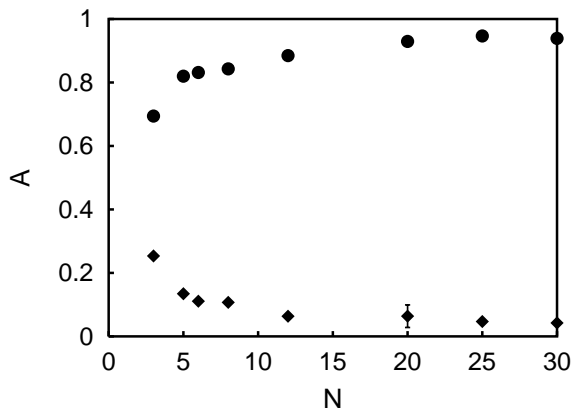


FIG. 11: Spectral weight of the *a*-type line (filled circles) and the *b*-type line (diamonds) for f-OCS@He<sub>N</sub>.

The general appearance of both quantities for f-OCS is closer to HCN than OCS, due to the presence of an *a*-type and a *b*-type line, with the spectral weight of the latter decaying with increasing  $N$ . However, at variance with HCN, the *a*-type line for large  $N$  approaches an energy significantly smaller than the gas-phase value,  $2B_0$ . Taking the value at  $N = 30$  as an estimate (very likely an overestimate, see Section III.A) of the asymptotic value, we obtain  $\Delta \simeq 0.33$ , which is close to—and somewhat smaller than—the value of OCS.

The *a*-type line of f-OCS shows a minimum at  $N = 6$  or 7, i.e. at a smaller size than OCS. As shown in Fig. 12 already for  $N = 8$  there is a significant He density all around the molecule, which is presumably responsible for the turnaround of the  $B$  value (although the relation between density profiles and turnaround of the  $B$  value could be not so straightforward for f-OCS, due to the

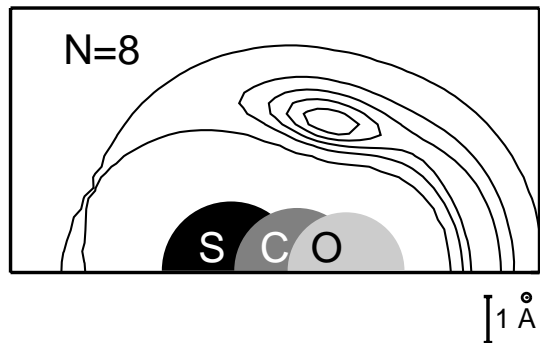


FIG. 12: Contour plot of the helium density profile of f-OCS@He<sub>8</sub>.

residual spectral weight in the *b*-type line). Regardless of the implications for the turnaround, we stress that the significant difference between the density profiles between f-OCS and OCS (see Fig. 12 and Fig. 2 for  $N = 8$ ) implies a significantly different *amount of adiabatic following*. The fact that the  $\Delta$  values of f-OCS and OCS are nevertheless very similar, indicates that the anisotropy of the potential, rather than the dynamical regime implied by the gas-phase inertia, is mainly responsible for the renormalization of the rotational constant upon solvation.

Similar conclusions hold for f-HCN as well. The energy of the lowest rotational excitation with  $J = 1$  is shown in Fig. 13 as a function of  $N$ . Already for  $N = 3$  the spectral weight of this excitation exceeds 90 percent, and in this respect f-HCN is closer to OCS than to HCN (i.e. the spectrum looks that of a linear rotor for  $N \geq 3$ ). However as far as the value of  $\Delta$  is concerned, the effect of fudging the gas-phase inertia is very small.

In order to estimate the asymptotic limit of the rotational constant, we assume that it is given by the value at the largest-size cluster simulated ( $N = 25$ ), noting that the evolution of  $B(N)$  in Fig. 13 is nearly flat for  $N \geq 12$  (for HCN, this assumption would give a very good agreement with the experimental nano-droplet value, see Fig. 8). This gives  $\Delta = 0.90$  for f-HCN, close to—and somewhat higher than—the value 0.81 measured in HCN [23].

Our findings indicate that the potential alone has a dominant role in establishing the value of  $\Delta$ , at least in the range of physical parameters appropriate to the linear molecules studied here. Furthermore, the effect of reducing the molecular inertia while keeping the PES fixed is to slightly *decrease* the  $\Delta$  value. This result, in agreement with an experimental study of HCN and DCN [23], contradicts the empirically established correspondence between light rotational inertia and large  $\Delta$  values. We conclude that such a correspondence is due,

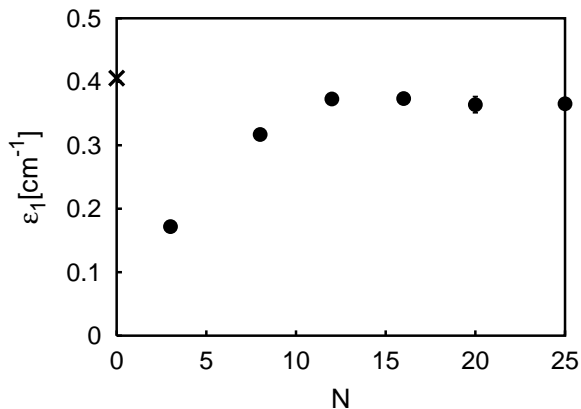


FIG. 13: Rotational energies of f-HCN@He<sub>N</sub> as a function of the cluster size. The cross at  $N = 0$  shows the fictitious value of  $2B_0$ .

to a large extent, to the generally small anisotropy of the interaction between light rotors and Helium—an accidental effect, as far as the rotational dynamics of the solvated molecule is concerned. Within this picture, the behavior of N<sub>2</sub>O is not an *anomalous* case, but merely a consequence of the stronger stiffness and anisotropy of the N<sub>2</sub>O-He potential with respect to, say, OCS or CO<sub>2</sub>.

We finally note that a previous calculation for SF<sub>6</sub> with a fictitiously small gas-phase inertia would support the opposite conclusion that, for given interaction with the solvent, a lighter molecule would have a larger value of  $\Delta$  [32]. While this result could shed some doubts on the generality of the conclusions drawn from the analysis of a few *linear* molecules, we believe that the calculations of Ref. 32 probably deserve further analysis because they were obtained using a fixed-node approximation, whose accuracy is not warranted especially for light rotors [24].

## CONCLUSIONS

Quantum Monte Carlo simulations, in conjunction with high-quality inter-particle potentials, have reached a remarkable degree of accuracy for the calculation of the rotational dynamics of molecules solvated in He. Using the RQMC method, we have studied the evolution of the rotational excitations with the number  $N$  of solvent He atoms for a prototype heavy rotor, OCS, and a prototype light rotor, HCN (for OCS, preliminary results have already been presented in Ref. 8). The size range explored, larger than presently attained with number-selective IR and/or MW spectroscopy, allows us to draw a series of conclusions on the approach of the rotational constant to its asymptotic value in the nano-droplet limit. Our results entail a substantial revision, both quantitative and qualitative, of the common view that the asymptotic

limit would be essentially determined by the amount of adiabatic following and that—at least for heavy rotors—it would be reached well before completion of the first solvation shell.

The rotational constant of OCS, after the undershoot of the nano-droplet value and the turnaround which signals the onset of superfluidity, crosses again its asymptotic limit at  $N = 12$ ; moreover, starting with the beginning of the second solvation shell around  $N \approx 20$ , it develops a further structure with an extremely broad maximum, and a possible hint of a (final?) decrease only seen at the largest size we studied,  $N = 50$ . This feature, which parallels similar findings for CO<sub>2</sub> and N<sub>2</sub>O, definitely supports *slow* convergence to the nano-droplet value. A strikingly different behavior is found for HCN. In this case, a linear-rotor-like spectrum is found for  $N$  larger than 10, and the resulting rotational constant stays constant in a wide range (say 15 to 50), with a value close to the measured value in the nano-droplet limit. This result contradicts the expectation of a slow convergence to the asymptotic limit (determined by coupling of molecular rotation with well-developed bulk-like excitations of the solvent) as a general property of light rotors. Indeed, a behavior very similar to that illustrated here for HCN was found for another light rotor, namely CO. It would be tempting to propose that *fast* convergence to the nano-droplet limit is a general rule for light rotors. However, preliminary experimental results [33] seem to indicate that, for CO, the asymptotic limit is significantly lower than inferred from the nearly constant value of the rotational constant in the size range from a dozen to a few tens He atoms. The possibility of defining a general trend for light rotors thus deserves further investigation.

In order to establish the relative importance of the bare molecular inertia and of the strength and anisotropy of the He-molecule interaction in determining the approach of the rotational dynamics to the nano-droplet regime, we have also performed computer experiments in which the molecular inertia was intentionally modified. To this end, we have considered two *fudged* molecular species, f-OCS and f-HCN, *i.e.* OCS and HCN with fictitiously small and fictitiously large values of the gas-phase rotational constant, respectively (appropriate in fact to the *other* molecule). Perhaps the most important feature which was attributed to the predominant role of the bare molecular inertia is the amount of renormalization of the gas-phase rotational constant,  $B$ , upon solvation: the strong (weak) reduction of  $B$  observed for heavy (light) rotors was attributed to the large (small) amount of adiabatic following. Our results indicate that the fractional reduction of the gas-phase rotational constant upon solvation is slightly *stronger* for f-OCS than for true OCS, despite the obvious fact that adiabatic following is much larger for the latter. Likewise, the reduction calculated for f-HCN is somewhat *weaker* for f-HCN than for true HCN. The same trend was experimentally observed, with a smaller

variation of  $B_0$ , in a comparative study of HCN and DCN [23]. This clearly shows that it is the strength and anisotropy of the He-molecule interaction, rather than the bare molecular inertia, which is mainly responsible for the renormalization of the rotational constant in the nano-droplet regime. In this perspective, the classification into heavy and light rotors thus retains its validity only to the extent that heavier molecules tend to have stronger and more anisotropic interactions with He.

We thank Giacinto Scoles for many fruitful discussions. Part of the calculations presented in this work were done thanks to the *Iniziativa Calcolo Parallelo* of the Italian Institute for the Physics of Matter (INFM).

---

\* Electronic address: paolini@sissa.it

† Electronic address: fantoni@sissa.it

‡ Electronic address: moroni@caspur.it

§ Electronic address: baroni@sissa.it

- [1] S. Grebenev, J.P. Toennies, and A.F. Vilesov, *Science* **279**, 2083 (1998).
- [2] J. Tang, Y.J. Xu, A.R.W. McKellar, and W. Jäger, *Science* **297**, 2030 (2002).
- [3] S. Baroni and S. Moroni, in *Quantum Monte Carlo Methods in Physics and Chemistry*, edited by P. Nightingale and C.J. Umrigar. NATO ASI Series, Series C, Mathematical and Physical Sciences, Vol. 525, (Kluwer Academic Publishers, Boston, 1999), p. 313, also available at cond-mat/9808213.
- [4] S. Baroni and S. Moroni, *Phys. Rev. Lett.* **82**, 4745 (1999).
- [5] D. Blume, M. Lewerenz, P. Niyaz, and K. B. Whaley, *Phys. Rev. E* **55**, 3664 (1997).
- [6] S. Moroni, A. Sarsa, S. Fantoni, K.E. Schmidt, and S. Baroni, *Phys. Rev. Lett.* **90**, 143401 (2003).
- [7] F. Paesani, A. Viel, F.A. Gianturco, and K.B. Whaley, *Phys. Rev. Lett.* **90**, 73401 (2003).
- [8] S. Moroni and S. Baroni, *Comp. Phys. Comm.* in press (2005).
- [9] Y. Kwon, P. Huang, M. V. Patel, D. Blume, and K. B. Whaley, *J. Chem. Phys.* **113**, 6469 (2000).
- [10] J.P. Toennies and A.F. Vilesov, *Angew. Chem. Int. Ed.* **43**, 2622 (2004).
- [11] J.M.M. Howson and J.M. Hutson, *J. Chem. Phys.* **115**, 5059 (2001).
- [12] T. Korona, H. L. Williams, R. Bukowski, B. Jeziorski and K. Szalewicz, *J. Chem. Phys.* **106**, 5109 (1997).
- [13] R. R. Toczyłowski, F. Doloresco, and S. M. Cybulski, *J. Chem. Phys.* **114**, 851 (2000).
- [14] F. Paesani and K.B. Whaley, *J. Chem. Phys.* **121**, 4180 (2004).
- [15] We have verified that the residual discrepancy visible in Fig. 6 of Ref. 14 can be removed by improving the convergence of the RQMC simulations with respect to the length of the quantum paths (*snakes*).
- [16] P. Cazzato, S. Paolini, S. Moroni, and S. Baroni, *J. Chem. Phys.* **120**, 9071 (2004).
- [17] J. E. Gubernatis and M. Jarrell, *Phys. Rep.* **269**, 135 (1996).
- [18] S. Moroni, N. Blinov and P.-N. Roy, *J. Chem. Phys.* **121**, 3577 (2004).
- [19] J. Tang, A. R. W. McKellar, F. Mezzacapo and S. Moroni, *Phys. Rev. Lett.* **92**, 145503 (2004).
- [20] Y. Xu, W. Jäger, J. Tang, and A. R. W. McKellar, *Phys. Rev. Lett.* **91**, 163401 (2003).
- [21] J. Tang and A. R. W. McKellar, *J. Chem. Phys.* **121**, 181 (2004).
- [22] E.W. Draeger and D.M. Ceperley, *Phys. Rev. Lett.* **90**, 065301 (2003).
- [23] A. Conjusteau, C. Callegari, I. Reinhard, K. K. Lehmann, and G. Scoles, *J. Chem. Phys.* **113**, 4840 (2000).
- [24] A. Viel and K. B. Whaley, *J. Chem. Phys.* **115**, 10186 (2001).
- [25] C. Callegari, A. Conjusteau, I. Reinhard, K. K. Lehmann, G. Scoles, and F. Dalfvo, *Phys. Rev. Lett.* **83**, 4108 (1999).
- [26] R. Zillich and K. B. Whaley, *Phys. Rev. B* **69**, 104517 (2004).
- [27] J. Tang, A.R.W. McKellar, *J. Chem. Phys.* **119**, 754 (2003).
- [28] F. Paesani and F. A. Gianturco, *J. Chem. Phys.* **116**, 10170 (2002).
- [29] S. Moroni, M. Botti, S. De Palo and A. R. W. McKellar, *J. Chem. Phys.*, in press.
- [30] S. Baroni and S. Moroni, *Chem. Phys. Chem.*, in press (2005).
- [31] M. V. Patel, A. Viel, F. Paesani, P. Huang and K. B. Whaley, *J. Chem. Phys.* **118**, 5011 (2003).
- [32] E. Lee, D. Farrelly and K. B. Whaley, *Phys. Rev. Lett.* **83**, 3812 (1999).
- [33] M. Havenith, private communication.